Journal of Hydrology 511 (2014) 320–334

Contents lists available at ScienceDirect

Journal of Hydrology

journal homepage: www.elsevier.com/locate/jhydrol

Groundwater flows in weathered crystalline rocks: Impact of piezometric variations and depth-dependent fracture connectivity

N. Guihéneuf [a,b,*], A. Boisson [a], O. Bour [b], B. Dewandel [c], J. Perrin [a,1], A. Dausse [a,2], M. Viossanges [a], S. Chandra [d], S. Ahmed [d], J.C. Maréchal [c]

[a] BRGM, D3E, New Resource & Economy Unit, Indo-French Center for Groundwater Research, Uppal Road, 500007 Hyderabad, India
[b] OSUR, Géosciences Rennes, UMR6118 CNRS – Université de Rennes 1, 35042 Rennes Cedex, France
[c] BRGM, D3E, New Resource & Economy Unit, 1039, rue de Pinville, 34000 Montpellier, France
[d] National Geophysical Research Institute, Indo-French Center for Groundwater Research, Uppal Road, 500007 Hyderabad, India

ARTICLE INFO

Article history:
Received 14 November 2013
Received in revised form 24 January 2014
Accepted 27 January 2014
Available online 4 February 2014
This manuscript was handled by Peter K. Kitanidis, Editor-in-Chief, with the assistance of Jean-Raynald de Dreuzy, Associate Editor

Keywords:
Fractures connectivity
Groundwater flow
Sustainable groundwater resources
Hard rock
Semi-arid region
Vulnerability

SUMMARY

Groundwater in shallow weathered and fractured crystalline rock aquifers is often the only perennial water resource, especially in semi-arid region such as Southern India. Understanding groundwater flows in such a context is of prime importance for sustainable aquifer management. Here, we describe a detailed study of fracture properties and relate the hydraulic connectivity of fractures to groundwater flows at local and watershed scales. Investigations were carried out at a dedicated Experimental Hydrogeological Park in Andhra Pradesh (Southern India) where a large network of observation boreholes has been set up. Twenty-height boreholes have been drilled in a small area of about 18,000 m^2 in which borehole loggings and hydraulic tests were carried out to locate the main flowing fractured zones and investigate fractures connectivity. Several hydraulic tests (nineteen slug tests and three pumping tests) performed under two water level conditions revealed contrasting behavior. Under high water level conditions, the interface including the bottom of the saprolite and the first flowing fractured zone in the upper part of the granite controls groundwater flows at the watershed-scale. Under low water level conditions, the aquifer is characterized by lateral compartmentalization due to a decrease in the number of flowing fractures with depth. Depending on the water level conditions, the aquifer shifts from a watershed flow system to independent local flow systems. A conceptual groundwater flow model, which includes depth-dependent fracture connectivity, is proposed to illustrate this contrasting hydrological behavior. Implications for watershed hydrology, groundwater chemistry and aquifer vulnerability are also discussed.

1. Introduction

Groundwater in weathered and fractured crystalline aquifers constitutes the only available water resource in many areas, especially in arid and semi-arid regions (Gustafson and Krásný, 1994). In Southern India, since the Green Revolution of the 70s, the overexploitation of groundwater resources for agriculture, particularly to irrigate rice crops, has led to water table depletion (Shah et al., 2003; Maréchal et al., 2006; Reddy et al., 2009; Dewandel et al., 2010; Maréchal, 2010; Perrin et al., 2011a), and the deterioration of groundwater quality, especially fluoride contamination (Ayoob and Gupta, 2006; Perrin et al., 2011b; Pettenati et al., 2013). Understanding groundwater flows and transport processes in such a context is therefore of prime importance to reach a sustainable management of groundwater resources.

Fractured crystalline aquifers composed mainly of metamorphic and igneous rocks are subject to weathering processes, especially chemical weathering that leads to a typical profile with variable hydraulic conductivity and porosity (Larsson, 1984; Foster, 1984; Jones, 1985; Acworth, 1987; Houston and Lewis, 1988; Wright, 1992; Anand and Paine, 2002; Dewandel et al., 2006). Several studies have focused on the hydraulic properties of such systems and hydrogeological conceptual models have been proposed

* Corresponding author at: OSUR, Géosciences Rennes, UMR6118 CNRS – Université de Rennes 1, 35042 Rennes Cedex, France. Tel.: +33 223235586.
E-mail address: nicolas.guiheneuf@univ-rennes1.fr (N. Guihéneuf).
[1] Present address: BRGM, D3E, GDR, 3, Av Claude Guillemin, 45060 Orléans, France.
[2] Present address: Hydrosciences, UMR 5569 – Université de Montpellier 2, Place E. Bataillon, 34095 Montpellier Cedex 5, France.

http://dx.doi.org/10.1016/j.jhydrol.2014.01.061
0022-1694/

that include from top to bottom: weathered rock including the saprolite, fractured rock and fresh or un-fractured rock (Larsson, 1984; Chilton and Foster, 1995; Taylor and Howard, 2000; Maréchal et al., 2004; Wyns et al., 2004; Dewandel et al., 2006; Banks et al., 2009). Groundwater flow in such media is localized in a small part of the rock volume and is mainly controlled by fracture connectivity (National Research Council, 1996; Paillet, 1998; Day-Lewis et al., 2000; Le Borgne et al., 2006). Connectivity is dependent on the geometrical properties of the fracture network, i.e. the distribution of fracture lengths, fracture orientations as well as fracture density (Bour and Davy, 1998; de Dreuzy et al., 2001). Unfortunately, these geometrical properties are often difficult to estimate in the field, especially on a large-scale, since large amounts of data are required (National Research Council, 1996). An alternative approach consists of using a continuum approach (Courtois et al., 2010; Dewandel et al., 2012) to simplify these complex systems and upscale the hydraulic parameters. However, such continuum approaches usually assume that the system is relatively well-connected, at least on a large enough scale, to allow the point to point measurements of hydraulic properties to be regionalized.

In a relatively stable tectonic context like Southern India, fractures are mainly dilating fractures or joints (mode 1 opening-mode) (National Research Council, 1996) which in general provide permeability for groundwater flow. Near horizontal dilating fractures at shallow depths are commonly known as sheeting joints or exfoliation joints in intrusive igneous rocks such as granite (Dale, 1923; Twidale, 1973; Bahat et al., 1999). One particularity of these fractures is their development parallel to the surface of the plutonic body. From a structural point of view, it is generally acknowledged that fracture frequency decreases with depth in the first hundred meters below ground surface (Dale, 1923; Twidale, 1973). Several authors (Howard et al., 1992; Briz-Kishore, 1993; Dewandel et al., 2006) reported that the main flowing fractured zone is located in the upper part of the bedrock, just below the saprolite. Since fracture density is expected to decrease with depth (Maréchal et al., 2004; Dewandel et al., 2006), fracture connectivity should play an important role in groundwater flow, and may control fluxes at the watershed scale, at least at a given depth. However, the relationship between the geometrical specificities of fractures and groundwater flows at local and watershed scales, especially at depth, is not clearly understood.

Here, we describe a detailed study of geometrical and hydraulic properties of fractures that was carried out at different depths and on different scales to improve the conceptual model of groundwater flow in weathered crystalline aquifers at the site scale. This study took advantage of the Experimental Hydrogeological Park in Southern India where a set of observation boreholes have been drilled for scientific purposes. Several hydrogeological experiments at borehole and aquifer scales and under different hydrological conditions were done to estimate the hydraulic properties and main flow paths on the site. Finally, the implications of these results are discussed at watershed scale to investigate the consequences of fracture connectivity on watershed hydrogeology.

2. Hydrogeological context

2.1. Geological setting

The Experimental Hydrogeological Park (EHP) is situated near Choutuppal village in the Nalgonda district (Andhra Pradesh State, Southern India) 60 km to the south-east of Hyderabad (Latitude: 17°17′47″N; Longitude: 78°55′12″E) (Fig. 1). The EHP was developed by the French Geological Survey (BRGM) and the National Geophysical Research Institute (NGRI) on the campus of NGRI in Choutuppal. The site is included in the SOERE H + International hydrogeological sites network. The EHP is covered by sparse vegetation and characterized by a gentle slope towards the northeast of around 2%. The ground surface elevation measured at the center of EHP is about 365.5 meters above mean sea level. Numerous farmlands, including rice fields, with pumping boreholes belonging to farmers, are present around the EHP.

About 66% of the Andhra Pradesh State is composed of an Archean granitic and gneissic complex (Fig. 2). Locally, these formations may be intruded by dolerite dykes or quartz reefs (G.S.I., 1999, 2005; Perrin et al., 2011a; Dewandel et al., 2011). From a geomorphological viewpoint, the Nalgonda district is a gently undulating region with hummocky hills, boulders, ridges and inselbergs. The fracturing of granite is mainly characterized by dilating fractures. This kind of fracture displays specific characteristics and detailed descriptions of other sites in the world are given in Dale (1923), Jahns (1943), Twidale (1973), Bahat et al. (1999), Vidal Romaní and Twidale (1999), Hencher et al. (2011). It is generally accepted that dilating fracture can be slightly curved but are mostly horizontal, developing sub-parallel to the rock surface. Their spacing increases with depth from a few centimeters near the surface to a few meters, typically one to ten meters (Dale, 1923; Jahns, 1943). They can develop at up to one hundred meters depth (Jahns, 1943), and can display a lateral extension of more than one hundred meters (Hencher et al., 2011). These fractures may end in the fresh rock or by crossing other pre-existing fractures (Hencher et al., 2011). A few sub-vertical dilatant fractures can also be observed on several outcrops around EHP. Such outcrops which are relatively numerous and scattered over the watershed, can constitute isolated boulders extending into the saprolite or the granite surface. No evidence of faulting or tectonic activity has been observed in the area. The fracture orientations can be grouped into three families (Pira, 2009): N55-75, N130-155 and N165-175. Nevertheless, it remains difficult to relate or extrapolate such fracture orientations to bedrock fractures at depth.

The EHP consists of twenty-height boreholes of different depths (Table 1). The thickness of the saprolite, according to the information obtained from drilling, varies between thirteen to twenty-four meters. Note that some relatively fresh and very poorly fractured granite may be observed in few places within EHP. However, no boreholes have been drilled in these places. Six boreholes have been drilled into the saprolite (CH3-L, CH10-L, CH21, CH22, CH23 and CH24) at specific depths, not exceeding seventeen meters. Two boreholes cross cut the saprolite and the first eight meters of granite at about twenty-three meters depth (CH3-S and CH10-S). The other boreholes stop at fifty or seventy meters from the ground surface. All boreholes have been equipped with a plain casing extending into the saprolite. All of them were screened or open in front of the contact zone between the saprolite and fractured granite. Below the contact zone, all boreholes were uncased (i.e., open hole). Four boreholes into the saprolite (CH21 to CH24) were also uncased from the last two meters to allow specific experiments within the vadose zone. The boreholes configuration was chosen to allow characterizations focused on the lateral hydraulic connectivity of fractures.

The typical geological profile obtained in the EHP by drilling cuttings analysis, follows the lithological description by Dewandel et al. (2006) which from top to bottom consists of:

- Red soil from the first decimeters to the first meter: rich in iron and/or aluminum oxides.
- Sandy regolith from about 1–3 m deep: yellowish color, sandy-clay composition, sandy texture with a lot of quartz grains.
- Saprolite from about 3 to 13–24 m deep, derived from in situ weathering of granite: yellowish to brownish color, coarse sand-size clasts texture and laminated structure. This horizon exhibits preserved fractures.

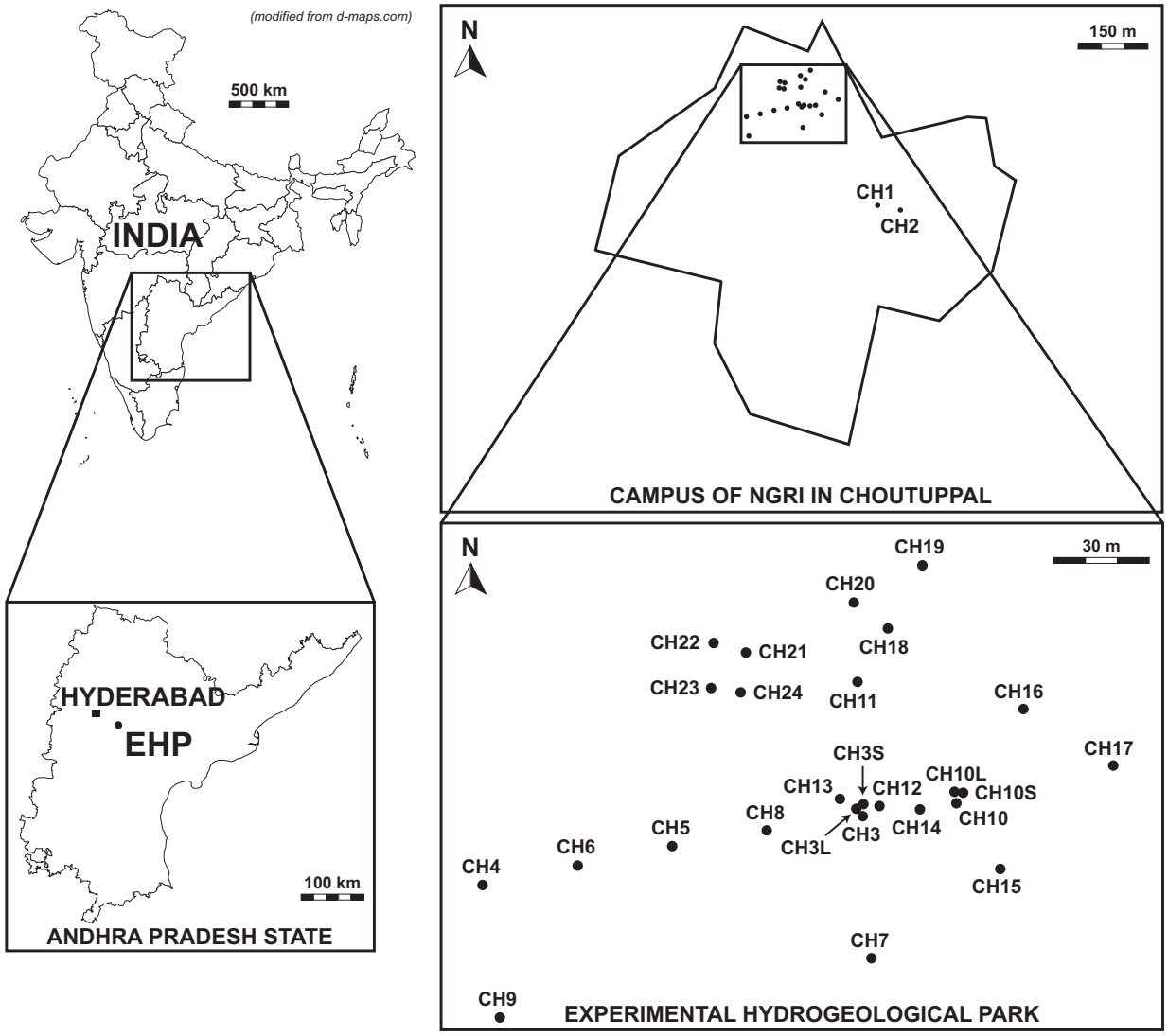

Fig. 1. Location of the Experimental Hydrogeological Park (EHP) in Andhra Pradesh State, Southern India. On the right hand side, the location of the NGRI field campus is shown with the boreholes network.

– Granite mainly constituted of quartz, potassium feldspars and biotite. Quartz veins, iron oxide and chlorite are also present. The upper part of the granite is highly weathered and fractured but the fracture frequency decreases rapidly with depth.

As a complement to the geological observations, some Electrical Resistivity Tomography profiles were performed at the EHP to image the possible presence of geological heterogeneities other than fractures in the sub-surface. Several geophysical cross-sections were obtained by using a Wenner-Schlumberger configuration. In particular, two ERT profiles of 450 m length crossing the EHP boreholes in west-east and south-north directions are presented in Fig. 3. These electrical resistivity profiles show an increase in resistivity with depth that more or less follows the weathering profile. Low resistivity values (<500 Ohm m) globally correspond to the saprolite while high resistivity values (>500 Ohm m), correspond to the granite. The interface between the saprolite and granite was determined from geological logs and is represented by dotted lines in Fig. 3. The electrical resistivity profiles did not reveal the presence of any vertical geological heterogeneity (dolerite dyke or quartz reef), but show that the thickness of the saprolite varies from place to place and increases northward.

2.2. Hydrological setting

The Andhra Pradesh region is characterized by a semi-arid climate controlled by monsoons. The rainy season occurs from June to November and is composed of south-west and north-east monsoons. The south-west monsoon from June to September generally constitutes 80% of the rainfall. During the rainy season, a temporary streams network may appear in the EHP. Nevertheless, surface streams are most of the time absent, thus highlighting the role of groundwater flow in watershed hydrology. The mean annual rainfall in the Choutuppal area is 693 mm and the mean annual temperature is 28 °C. The dry season occurs from December to May with a maximum temperature of 45 °C.

In Andhra Pradesh, groundwater constitutes the main water resource for rural communities. To understand the functioning of these aquifers, various hydraulic parameters were determined in previous studies (Maréchal et al., 2003, 2004; Dewandel et al., 2006, 2011, 2012) from slug tests and pumping tests analysis. The mean equivalent hydraulic conductivity was between 10^{-6} and 10^{-4} m s^{-1} with a vertical anisotropy ($K_r/K_z = 10$; Maréchal et al., 2003, 2004).

The changes in the water level in the CH3 borehole are

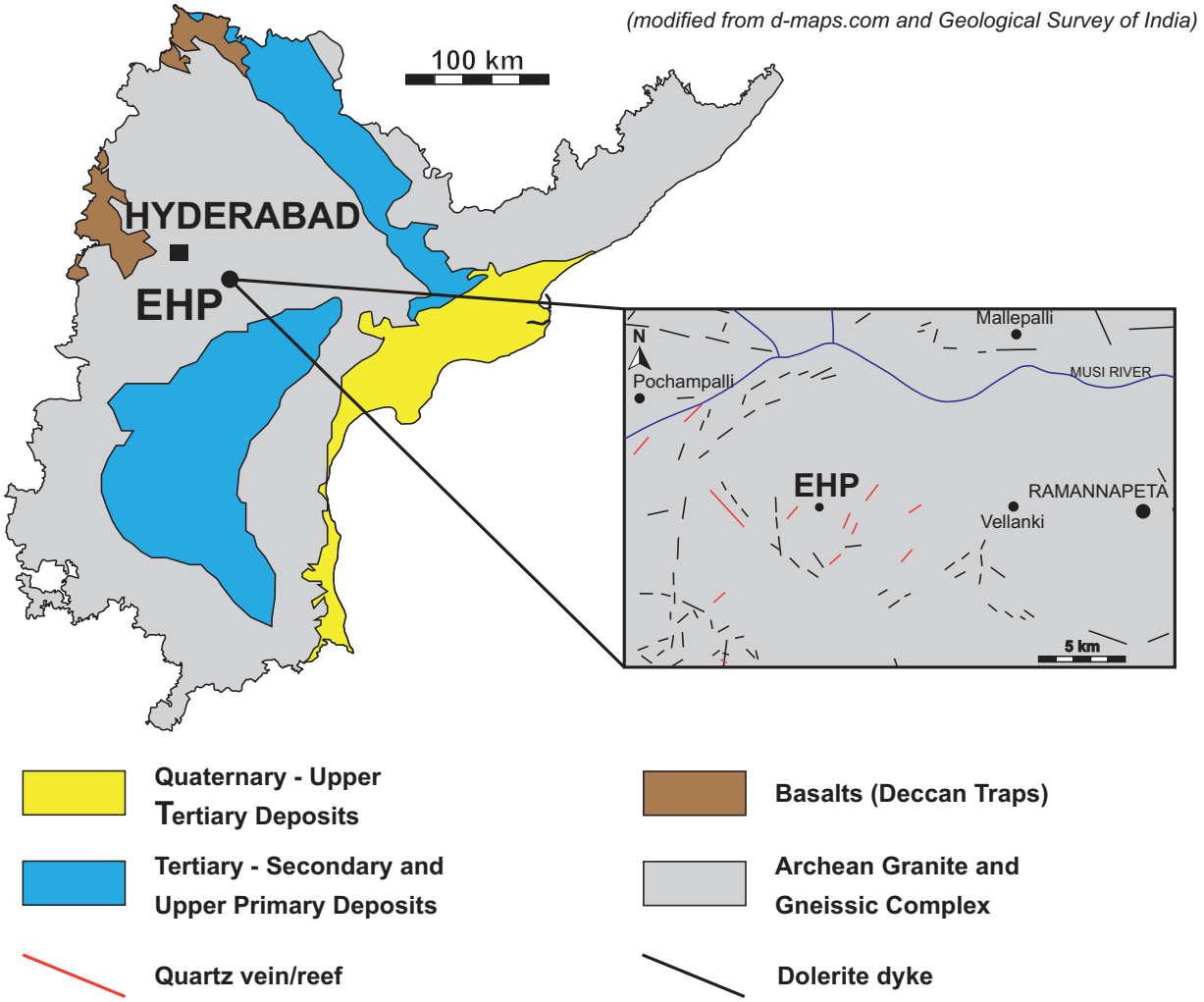

Fig. 2. Geological map of Andhra Pradesh, Southern India. Zoom represents the part of Nalgonda district in Andhra Pradesh where EHP is located.

compared with the geological log in Fig. 4. This hydrograph shows that during four years, only one monsoon significantly contributed to recharge the aquifer. After this significant recharge, the water level was above the granite, extending into the saprolite, for only a few months. Because of intensive pumping in the area surrounding the EHP, the saprolite remains unsaturated for most of the time. The spatial variations of the piezometric levels at the watershed scale are shown in Fig. 5. Two piezometric maps were drawn up under contrasting conditions, namely when the saprolite was partially saturated and when the water levels were quite low. Both piezometric maps were compiled in the dry seasons, therefore with no influence from rainfall recharge. The first one, under high water level conditions, was based on measurements carried out in June 2011 just before the beginning of the monsoon. The second one, under low water level conditions, was based on measurements performed in January 2013. The piezometric levels were measured four hours after irrigation pumping had stopped in order to avoid most of the local perturbations due to pumping. The piezometric map of 2011 shows a continuous hydraulic gradient indicating groundwater flow towards the north of the watershed that more or less follows the topography. Although the impact of the farmers pumping boreholes in the watershed during 2011 cannot be clearly identified, the piezometric level has globally decreased due to overexploitation. The piezometric map of 2013, when the saprolite was unsaturated, presents larger hydraulic gradient variations. In particular, the impact of pumping is clearly and readily apparent in a few places and no general groundwater flow direction can be defined at the watershed scale. This suggests that, when the water level is low, groundwater flows are restricted to the sub-compartments at greater depths. This is partly due to localized pumping but in some places the very sharp hydraulic variations also suggest a discontinuous medium (Fig. 5) which may result from a decrease in fracture connectivity with depth. Hereafter, we focus on the impact of fracture connectivity and water level conditions on groundwater flows at EHP.

3. Methodology

We characterized the groundwater hydrology and fracture connectivity at EHP by using a combination of methods involving borehole logging and hydraulic tests. The main permeable fractures were located by logging the fluid properties using an OTT probe (Temperature, Specific Conductivity, pH, Dissolved Oxygen and Redox Potential) and CTD divers (Temperature and Specific Conductivity). Both instruments provide measurements with an accuracy of ±0.1 °C for the temperature. Borehole logging was done sufficiently slowly to provide measurements every ten to twenty centimetres. Repeatability of the measurements has been systematically checked in all boreholes. The main permeable fractures were located by logging temperature in all EHP boreholes under ambient conditions (i.e. flowing naturally) as thermal anomalies

Table 1
Boreholes characteristics of the Experimental Hydrogeological Park in Choutuppal (Andhra Pradesh, Southern India). Boreholes location is provided in the UTM projected coordinate system. Borehole depth and casing depth are given in meters below ground surface.

Name of borehole	*X* (m)	*Y* (m)	Elevation (m amsl)	Borehole depth (m bgs)	Casing depth (m bgs)	Estimated saprolite's thickness (m)
CH1	279075.05	1913316.12	365.69	73.20	23.90	24.00
CH2	279120.68	1913296.32	366.31	73.20	18.75	19.00
CH3	278906.31	1913534.27	365.63	50.30	14.20	14.70
CH3-L	278904.34	1913535.85	365.69	14.70	14.70	14.50
CH3-S	278906.66	1913536.81	365.58	22.80	14.60	14.70
CH4	278787.66	1913518.59	367.45	73.20	15.70	14.45
CH5	278846.82	1913527.63	366.66	73.20	17.30	16.45
CH6	278817.45	1913523.11	366.96	73.20	17.25	17.35
CH7	278909.21	1913502.31	365.11	61.00	15.90	14.10
CH8	278876.59	1913531.05	366.11	61.00	17.30	18.00
CH9	278793.33	1913488.97	367.87	73.10	13.70	13.00
CH10	278935.78	1913537.14	364.97	70.00	18.00	17.00
CH10-L	278935.11	1913539.79	364.82	16.50	16.50	16.50
CH10-S	278937.64	1913539.51	364.79	22.80	16.70	16.00
CH11	278904.75	1913564.44	365.70	56.40	21.00	19.50
CH12	278911.70	1913536.59	365.57	56.40	15.00	14.80
CH13	278899.41	1913538.17	365.82	51.85	16.00	16.00
CH14	278924.14	1913535.76	365.24	56.40	18.30	17.90
CH15	278949.36	1913522.31	364.60	56.40	18.30	17.90
CH16	278956.63	1913558.42	364.61	56.40	17.30	15.20
CH17	278984.66	1913545.60	364.11	50.30	15.50	14.70
CH18	278914.12	1913576.32	365.57	50.30	19.80	21.35
CH19	278925.00	1913590.53	365.31	45.70	16.70	22.85
CH20	278903.75	1913582.33	365.42	54.85	23.00	22.85
CH21	278870.10	1913570.95	365.96	12.95	10.95	–
CH22	278860.12	1913573.08	365.95	7.70	5.80	–
CH23	278859.24	1913563.11	366.06	11.20	9.05	–
CH24	278868.41	1913562.03	366.08	4.30	2.15	–

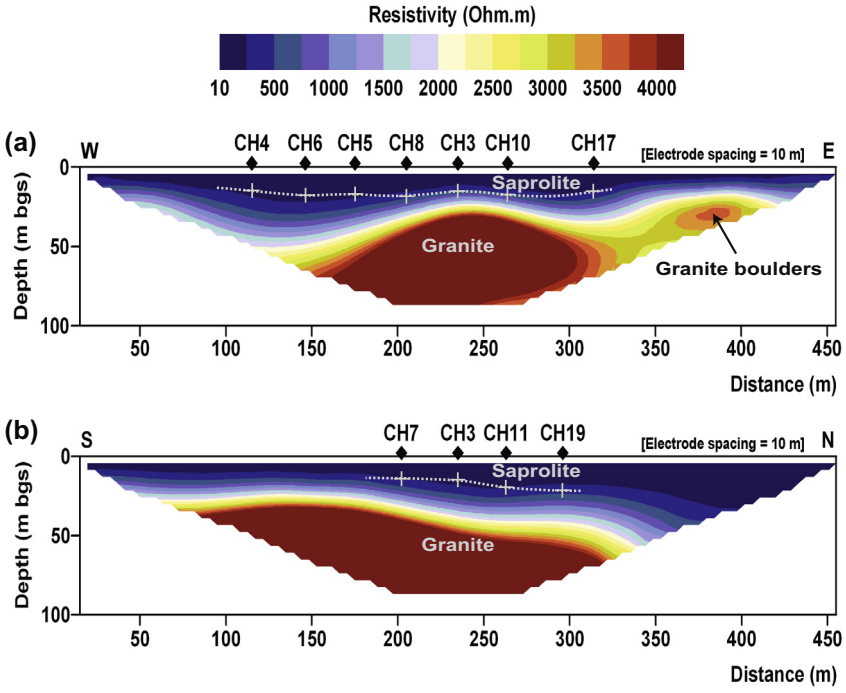

Fig. 3. Electrical Resistivity Tomography obtained in (a) west-east and in (b) south-north directions. Dotted line represents the interface between saprolite and granite obtained from geological logs.

in the geothermic gradient can indicate the presence of a permeable fracture (Drury, 1984; Keys, 1990; Chatelier et al., 2011). In particular, the temperature anomalies or gradients may be related to vertical water circulation between permeable fractures within boreholes (Klepikova et al., 2011). The precise location of a fracture can be determined with this simple method in the presence of significant vertical flow when no significant variations of rock thermal conductivity are apparent (i.e. typically in the same geological formation). Note that this method may not detect some permeable fractures, despite their presence in the borehole, if the flow is too small or if a temperature contrast is absent. Hereafter, we present a few typical examples of temperature logs obtained at EHP. In addition, camera investigations were carried out in some boreholes (CH3, CH10, CH11, CH12 and CH13) to correlate the locations of

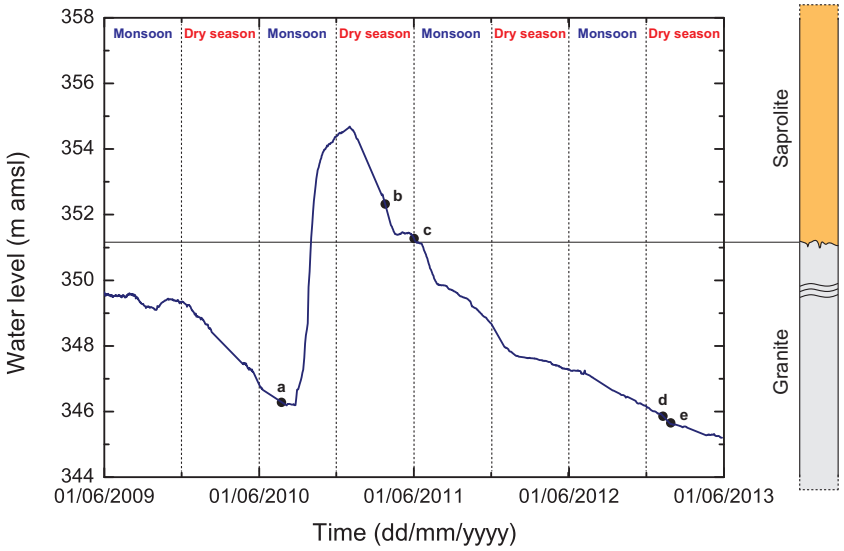

Fig. 4. Changes in water level in the CH3 borehole. A zoom on a typical geological log is shown on the right. The ground surface elevation for CH3 borehole is 366.4 m (amsl) (Table 1). Letters indicate: (a) the pumping test in CH3 at low water level conditions, (b) the pumping test in CH3 at high water level conditions, (c) the piezometric map of the watershed at high water level conditions, (d) the piezometric map of the watershed at low water level conditions and (e) the pumping test in CH11at low water level conditions. Fractures are represented by black curved lines.

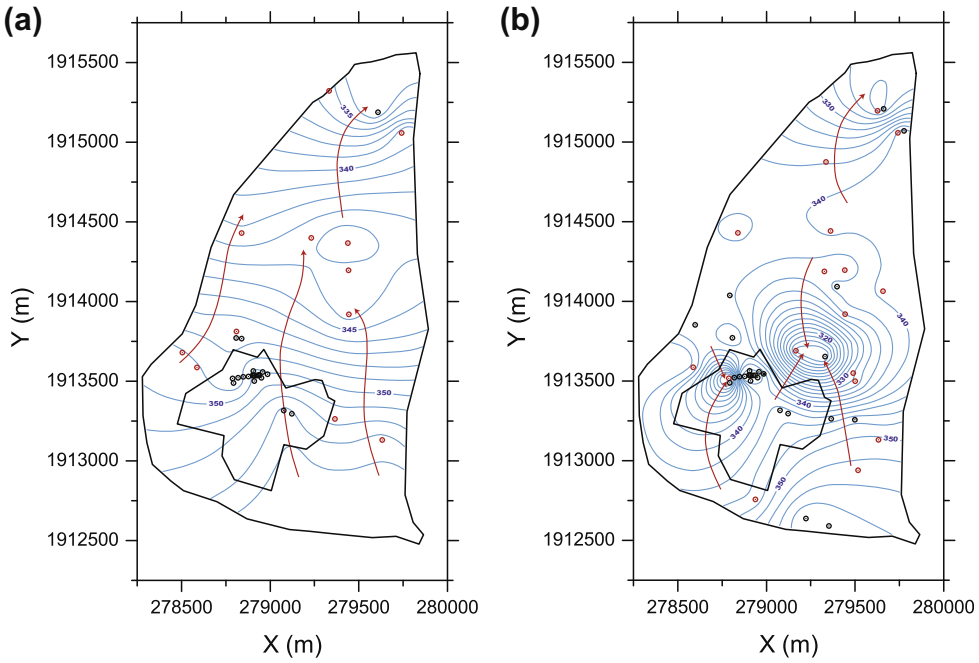

Fig. 5. Piezometric maps at the watershed scale, in the UTM projected coordinate system, obtained under two water level conditions but during dry seasons: (a) high water level map was obtained in June 2011 with 36 data points and (b) low water level map was obtained in January 2013 with 50 data points. Red arrows represent interpreted general groundwater flow paths and red points represent the farmers boreholes used for daily pumping. CH4, within EHP, is also used occasionally for groundwater resource since 2012. (For interpretation of the references to color in this figure legend, the reader is referred to the web version of this article.)

fractures and flowing fractures detected from temperature logs and hydraulic tests. Geophysical logs such as the single-point resistance and caliper logs would also have been useful but were not available at the time of the study.

The distribution of local transmissivity and hydraulic conductivity was obtained by performing slug tests in fifteen EHP boreholes and applying the Bouwer and Rice (1976) method for homogeneous confined and unconfined aquifers with fully or partially penetrating borehole. Three cycles of injection/pumping were carried out on the most transmissive boreholes and one on the low transmissive boreholes. These results were compared with those obtained when the saprolite or/and the top of the fractured granite was saturated, by performing the slug tests in four boreholes (CH3, CH5, CH10 and CH16) under two water level conditions. Note that this simply provided order-of-magnitude estimates of the hydrodynamic parameters as some phenomena, such as non-radial flows, would be overlooked (Shapiro and Hsieh, 1998). Nevertheless, slug tests analysis provides a first approach to characterize the variability of hydraulic properties in such heterogeneous media.

Several pumping tests were performed on-site to characterize the hydrodynamic properties and geometry of the aquifer. The first

pumping test, performed in CH3 when the water level was relatively low (19 m bgs, point a) in Fig. 4), lasted for three days with a discharge rate of 1.5 $m^3 h^{-1}$. Three observation boreholes (CH5, CH7 and CH8) and the pumping borehole, CH3, were monitored. The other boreholes had not been drilled at that time. The second pumping test in CH3 was performed when the water level was relatively high (13 m bgs, point b) in Fig. 4) for five days with a mean discharge rate of 6 $m^3 h^{-1}$. Variations of discharge rate were monitored from 6.2 to 5.6 $m^3 h^{-1}$. In this second case, drawdown was monitored in seventeen boreholes. A final pumping test was performed in CH11 when the water level was low (20 m bgs, point e) in Fig. 4). This pumping test was carried out for eleven days with a discharge rate of 0.5 $m^3 h^{-1}$, and monitored on the fifteen boreholes. All these data about the pumping tests are summarized in Table 2. The different discharge rates are related to the different transmissivities encountered for different water level conditions but also to the experimental design.

Pumping test analysis is often difficult, especially in fractured media where the complex geometry of the fractures network produces highly heterogeneous flow patterns (Barker, 1988; Le Borgne et al., 2004). The derivatives method was introduced by Bourdet et al. (1983) to improve pumping test interpretation. This method consists of identifying flow patterns on derivative drawdown curves (Bourdet et al., 1983; Gringarten, 2008; Renard et al., 2009) and defining a hydrodynamic conceptual model. In our case, drawdowns were normalized by pumping rate so that all the pumping tests could be compared. The derivative method was then applied to identify an appropriate and consistent model for data interpretation.

According to indications provided by the derivative method, we then applied the semi-analytical solution for confined and non-uniform aquifers developed by Butler (1988). This semi-analytical solution considers a pumping borehole which fully penetrates the aquifer and is located in the center of a circular disk of radius R, embedded in another reservoir of differing properties. The inner domain corresponding to the disk has a transmissivity T_1 [$m^2 s^{-1}$] and storage coefficient S_1 [–] while the outer domain has a transmissivity T_2 [$m^2 s^{-1}$] and storage coefficient S_2 [–].

4. Results

4.1. Borehole scale investigations

The temperature logs obtained at EHP revealed a few flowing fractured zones (typically one or two) on each borehole. Fig. 6 presents a typical temperature profile which varies from 30 °C to 31 °C. The local geothermal gradient, estimated from CH5 profile where very little and superficial temperature perturbations were observed, is relatively low (0.018 °C m^{-1}), but is in good agreement with another estimation (0.0114 °C m^{-1}) made by Akkiraju and Roy (2011) on the same site with deeper boreholes (about 300 m). These temperature logs also show one or two breaks that are characteristic of flowing fractured zones. The first zone is generally located near the bottom of the saprolite, in the first few meters of the upper part of the fractured granite. The second flowing fractured zone depends on the borehole location but can occur at the same depth in some boreholes, such as CH3, CH10 and CH12 (e.g. at about 25.5–27 m; Fig. 6). The locations of the flowing

Table 2
Characteristics of the different pumping tests.

Pumping borehole	Initial water level (m bgs)	Pumping rate ($m^3 h^{-1}$)	Duration (h)	Sampling rate (s)	Number of observation boreholes	Date of the test
CH3	19.18	1.5	70	30	3	July 2010
CH3	13.18	6	105	40	16	March 2011
CH11	19.81	0.5	261	30	14	January 2013

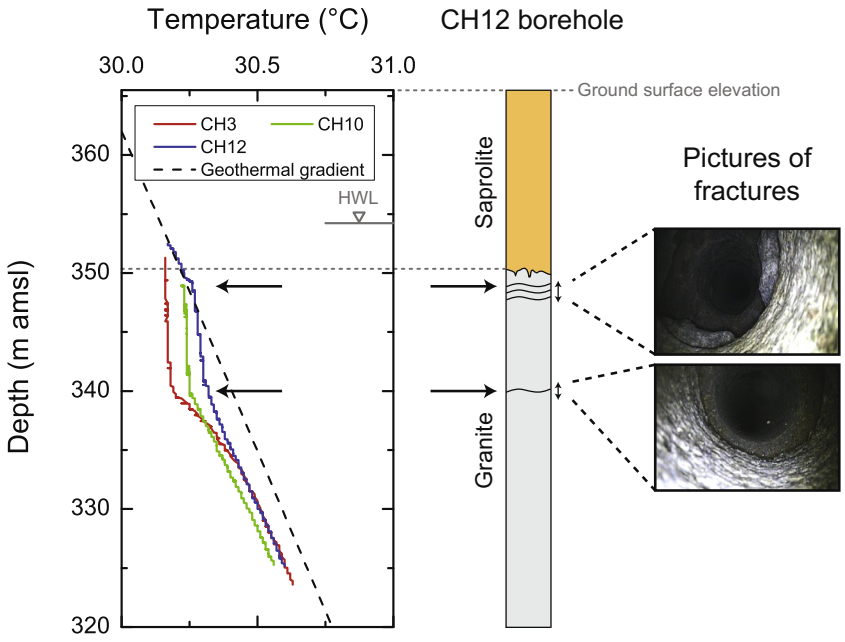

Fig. 6. Typical temperature profiles in the CH3, CH10 and CH12 boreholes carried out under high water level conditions (HWL), related to geological log and fractures observed by borehole camera in CH12. All temperature profiles were obtained under ambient conditions (i.e. flowing naturally). The geothermal gradient is presented in dotted line and was obtained from CH5 temperature profile. The mean surface temperature is about 28 °C. The main flowing fractures are indicated by black arrows.

fractured zones determined from the temperature logs agreed very well with the borehole camera investigations. In general, they occurred a few meters below the bottom of the saprolite. The number of flowing fractures that appeared to contribute significantly to flow was quite low, indicating that groundwater flow was localized in only a few fractures.

Slug tests analysis using the Bouwer and Rice method (1976) revealed a relatively high transmissivity variability ranging over three orders-of-magnitude from 1.7×10^{-7} to 5.4×10^{-4} m^2 s^{-1}. In addition, Table 3 presents all the results in terms of equivalent hydraulic conductivity. To obtain transmissivity, we simply multiply the hydraulic conductivity by the saturated length of the open borehole. Fig. 7 shows three typical data sets for the slug test injection obtained for boreholes CH8, CH10 and CH13 which displayed different hydraulic responses, ranging from high to low transmissivity. The fit to the data is in general quite good, except for the most transmissive responses where slight discrepancy may be observed, especially for late times (Fig. 7). The transmissivities of the first flowing fractured zone ($T_{\text{upper part}}$) were estimated from the difference between the transmissivities obtained under two water level conditions for the CH3, CH5 and CH10 boreholes (Table 3). The estimated mean transmissivities of the first flowing fractured zone, for these boreholes, were respectively 1.6×10^{-4} m^2 s^{-1}, 6.3×10^{-6} m^2 s^{-1} and 3.5×10^{-4} m^2 s^{-1}. Lower transmissivity values were obtained for deeper flowing fractures (Table 3). The estimated equivalent hydraulic conductivities for the entire dataset are within the range of values obtained in previous studies (Maréchal et al., 2004; Dewandel et al., 2006) with a geometric mean at EHP of 1.4×10^{-6} m s^{-1}.

Table 3
Transmissivities and equivalent hydraulic conductivities obtained by slug tests analysis with Bouwer and Rice (1976) methods. To obtain transmissivities, hydraulic conductivities were multiplied by the length of the open saturated boreholes.

Name of borehole	Initial water level (m bgs)	T (m^2 s^{-1})	K_{eq} (m s^{-1})	$T_{\text{upper part}}$ (m^2 s^{-1})
CH1	19.43	2.6×10^{-5}	5.4×10^{-7}	–
CH2	20.3	4.7×10^{-5}	8.8×10^{-7}	–
CH3	11.12	2.7×10^{-4}	8.0×10^{-6}	1.6×10^{-4}
	18.21	1.1×10^{-4}	3.3×10^{-6}	
CH5	18.77	6.5×10^{-6}	1.2×10^{-7}	6.3×10^{-6}
	21.32	1.7×10^{-7}	2.7×10^{-9}	
CH7	17.49	3.0×10^{-5}	6.9×10^{-7}	–
CH8	18.64	2.2×10^{-5}	5.2×10^{-7}	–
CH10	17.38	5.4×10^{-4}	1.0×10^{-5}	3.5×10^{-4}
	19.45	1.9×10^{-4}	3.8×10^{-6}	
CH11	18.19	1.1×10^{-4}	6.6×10^{-6}	–
CH12	18.03	1.9×10^{-4}	5.0×10^{-6}	–
CH13	18.32	7.0×10^{-5}	2.1×10^{-6}	–
CH14	17.71	2.3×10^{-5}	6.0×10^{-7}	–
CH15	16.85	1.3×10^{-4}	3.4×10^{-6}	–
CH16	16.63	1.6×10^{-4}	4.1×10^{-6}	–
	19.22	1.7×10^{-4}	4.5×10^{-6}	–
CH19	21.71	4.1×10^{-5}	1.7×10^{-6}	–
CH20	21.51	4.9×10^{-5}	1.5×10^{-6}	–
Geometric mean		5.3×10^{-5}	1.4×10^{-6}	7.1×10^{-5}

4.2. Pumping tests at the site scale

The pumping test carried out at CH3, when the water level was relatively high and the saprolite was partially saturated, led to significant hydraulic head variations in all nearby boreholes (Fig. 8a). Conversely, the pumping test performed at CH11 (Fig. 8b), when the water level was low, did not lead to hydraulic head variation in several boreholes (namely CH5, CH16, CH17, CH19 and CH20). Another pumping test performed in low water level conditions at CH3 cannot be fully compared with the previous tests as most of the boreholes had not been drilled at this time. Nevertheless, neither pumping tests at low water level led to any hydraulic head variations at CH5 whereas a reaction was observed under high water level conditions. Therefore, drawdowns appear to be dependent not only on the distance from the pumping borehole and the discharge rate, but also on the initial water level. This may be due to the dewatering under low water level conditions of better connected open fractures in the upper part of the granite. This suggests a decrease of the hydraulic connectivity with depth. Moreover, since the normalized drawdown was higher when the initial water level was low, this also implies that the transmissivity and/or storage coefficient also decreased with depth. Such observations rely on previous conceptual models of crystalline aquifer systems in semi-arid climate (e.g. Chilton and Foster, 1995; Taylor and

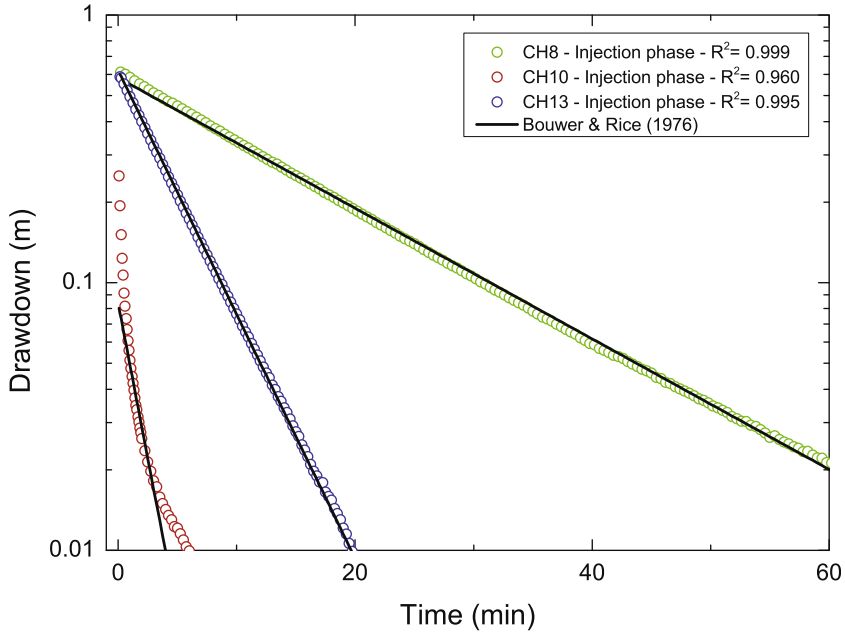

Fig. 7. Example of injection phase obtained under low water level conditions for slug tests in the CH8, CH10 and CH13 boreholes with interpretation according to the Bouwer and Rice (1976) method.

Howard, 2000; Maréchal et al., 2004; Dewandel et al., 2006), with saprolite contributing to storage whereas the fractured granite contributes to the transmissivity. This implies also that storativity will be quite reduced by the dewatering of the saprolite under low water level conditions.

Fig. 9 shows, in a log–log plot, the normalized drawdown and derivative curves obtained for the two pumping tests in CH3 which exhibited contrasting hydrodynamic behavior. Gray dots represent the specific drawdown and derivative obtained when the initial water level was low (19 m bgs), i.e. four meters below the bottom of the saprolite. The derivative analysis of drawdown reveals linear flow from 0 to 1 h, followed by a transitional flow for up to 5 h of the pumping test, similar to spherical flow. After 5 h of pumping, the derivative curve indicates a pseudo-radial flow.

The second pumping test at CH3, when the initial water level was about two meters above the bottom of the saprolite (13 m bgs), is represented as blue dots. Only the first part of the pumping test is shown since the first flowing fractured zone was dewatered after two days of pumping. In this case, the hydraulic response corresponded much more to a homogeneous system, as shown by the derivative analysis of drawdown (Fig. 9). This shows a linear flow up to 10 h and then a pseudo-radial flow from 10 to 50 h of pumping. Whatever the hydrodynamic behavior, the transmissivity obtained during the pumping test under high water level conditions was higher than that obtained when the water level was initially low. Note that although not shown (for clarity) in Fig. 9, the normalized drawdown derivative becomes equal to the derivative of the pumping test at low water level once the upper flowing fractured zone has been dewatered.

To complement the analysis, we used the semi-analytical solution by Butler (1988) described in the previous section (Fig. 9). The semi-analytical solution of Butler (1988) assumes radial flows, which is a limit of the model, but it could be used efficiently to estimate diffusivity contrast between both the inner and outer domains. This contrast of diffusivities between both domains can reproduce very well the drawdown evolution during pumping

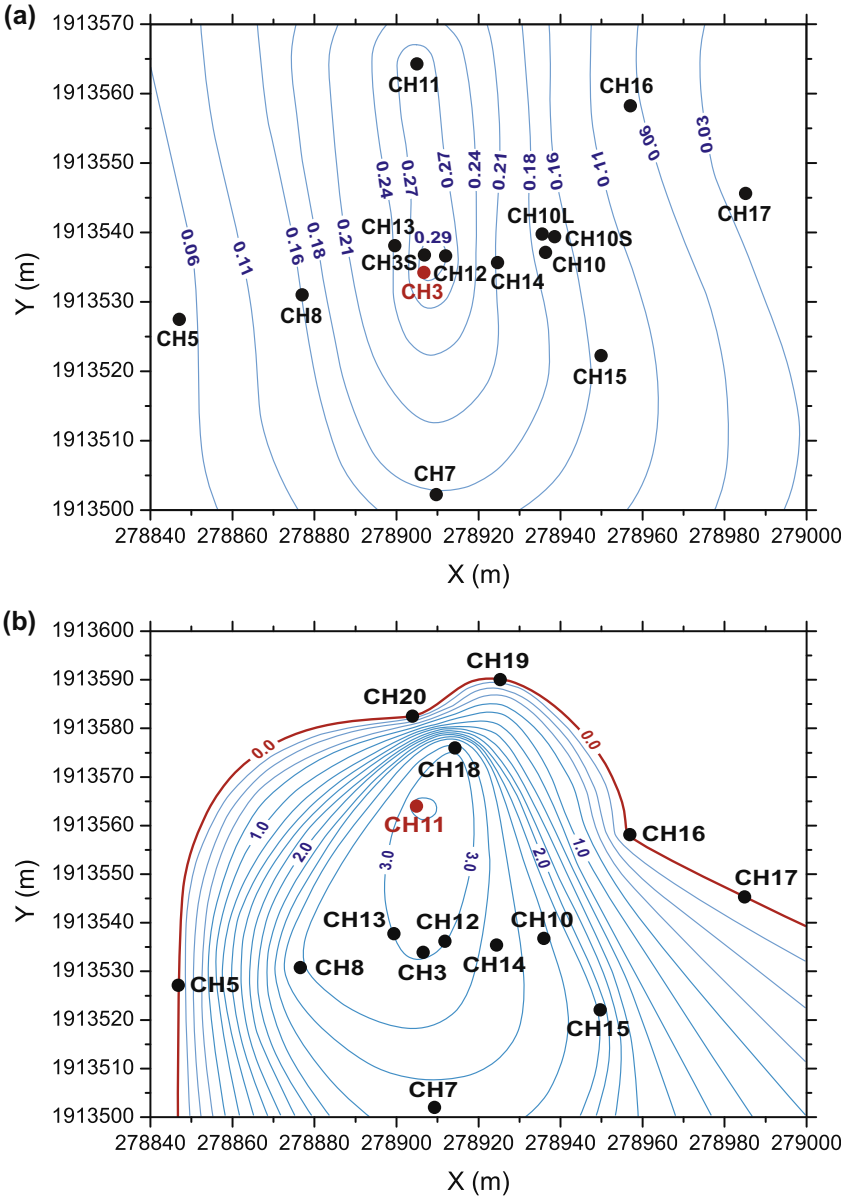

Fig. 8. Specific drawdown (m per m^3 h^{-1}) maps at the EHP, in the UTM projected coordinate system, obtained 1000 min after starting the pumping tests: (a) for CH3 pumping test performed at high water level and (b) for CH11 pumping test performed at low water level.

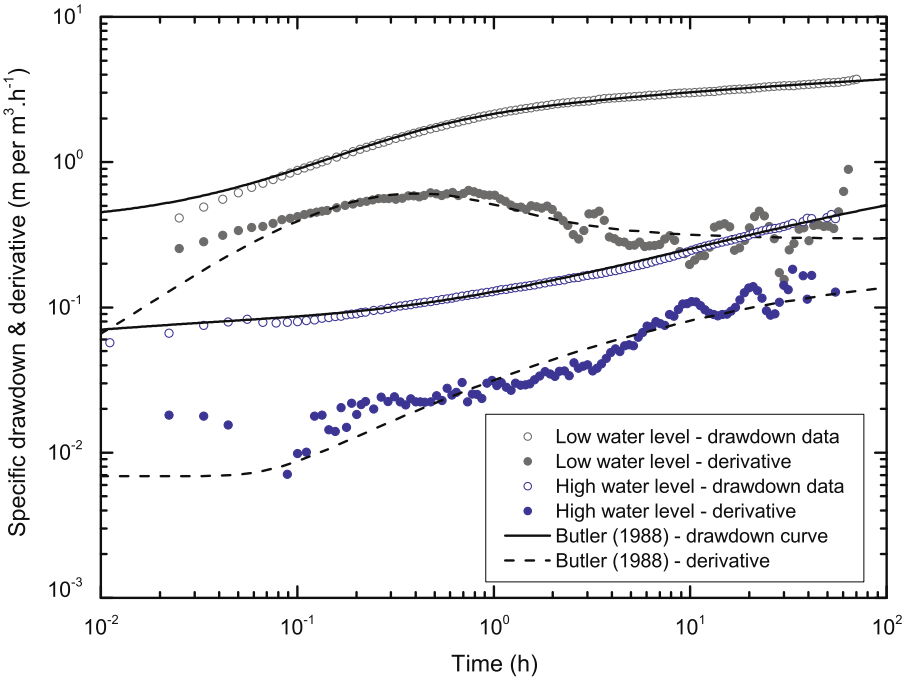

Fig. 9. Normalized drawdown and derivative data obtained for CH3 pumping borehole for the two pumping tests under low and high water level conditions. Butler (1988) model is represented by black line for drawdown curve and black dashed line for derivative curve.

tests. This solution was chosen because it also very consistent with the hydraulic compartmentalization observed under low water level conditions (Fig. 8b). Tables 3–5 show all the computed parameters for fitting drawdown and derivative curves. The transmissivities obtained for the pumping test performed under high water level conditions range between 1.5×10^{-3} and 3.2×10^{-3} $m^2\,s^{-1}$ for the inner domain and $1.3 \times 10^{-4}\,m^2\,s^{-1}$ for the outer domain. The transmissivities obtained for both pumping tests performed under low water level conditions range between 3.4×10^{-4} and $4.9 \times 10^{-4}\,m^2\,s^{-1}$ for the inner domain and between 4.9×10^{-5} and $9.4 \times 10^{-5}\,m^2\,s^{-1}$ for the outer domain. Modeling of the data set for all pumping tests also revealed variability of the storage coefficient values over a few orders of magnitude (Tables 3–5). Nevertheless this parameter remained relatively stable for each domain for a specific water level condition. Furthermore the diffusivity values estimated under low water level conditions were greater than under high water level conditions mainly because of a decrease in storativity with depth.

The radius of the inner domain was fixed at 45 m for the pumping test at high water level (Fig. 8b). The time for drawdown to reach the limit of the circular inner domain was about 3.7 min. For the pumping tests at low water level, it was necessary to fix the radius of the inner domain at 12 m to reproduce the data. Despite some uncertainty, this indicates that the extensions of the transmissive zones at depth are certainly much more limited.

All the results show that the bottom of the saprolite and the first fractured zone in the upper part of the granite are spatially well-connected and characterized by high transmissivity. At greater depths, the transmissivity and storage coefficients are lower. Moreover, the groundwater system is apparently more limited when the water level is below the upper part of the granite, resulting in a compartmented aquifer dependent on the water level conditions. For example, the boreholes CH4, CH6 and CH9 in the western part of EHP are highly influenced by farmers pumping whereas the other boreholes are not. In the following section, we provide a summary of our results and a comprehensive aquifer conceptual model at the site scale.

4.3. Results synthesis

The temperature loggings and borehole camera images show that the main flowing fractured zones are located just below the saprolite thus indicating hydraulic continuity in the lower saprolite and upper fractured zone. During high water level conditions, all boreholes were impacted by the pumping test in the CH3 borehole. Conversely, under low water level conditions, a certain number of boreholes were not impacted by the pumping tests performed in CH3 and CH11 thus indicating a segmentation of the aquifer and spatial discontinuity of deeper fractured zones. Fig. 10 shows a map of the site with the different boreholes and the temperature logs for the different compartments under low water level conditions. Four different compartments, which are not hydraulically connected, can be defined from previous hydraulic tests. The limits between the different compartments are not always clearly de-

Table 4
Computed parameters with R = 12 m for pumping test performed in the CH3 borehole at low water level conditions in July 2010.

Name of borehole	Distance from pumping borehole (m)	s_{max} (m)	T_1 ($m^2\,s^{-1}$)	S_1 (–)	T_2 ($m^2\,s^{-1}$)	S_2 (–)
CH3	Pumping borehole	5.6	4.9×10^{-4}	3.3×10^{-4}	7.5×10^{-5}	6.3×10^{-6}
CH5	59.87	No reaction	–	–	–	–
CH7	32.09	4.21	4.9×10^{-4}	5.3×10^{-4}	9.4×10^{-5}	2.8×10^{-7}
CH8	29.9	5.12	4.9×10^{-4}	5.7×10^{-4}	7.5×10^{-5}	7.1×10^{-7}
Geometric mean			4.9×10^{-4}	4.6×10^{-4}	8.1×10^{-5}	1.1×10^{-6}

Table 5
Computed parameters with $R = 45$ m for pumping test performed in the CH3 borehole at high water level conditions in March 2011.

Name of borehole	Distance from pumping borehole (m)	s_{max} (m)	T_1 ($m^2 s^{-1}$)	S_1 (–)	T_2 ($m^2 s^{-1}$)	S_2 (–)
CH1	275.8	No reaction	–	–	–	–
CH3	Pumping borehole	4.67	3.2×10^{-3}	1.4×10^{-3}	1.3×10^{-4}	6.3×10^{-3}
CH3-L	2.53	0.91	2.7×10^{-3}	5.6×10^{-3}	1.3×10^{-4}	5.6×10^{-3}
CH3-S	2.57	2.6	2.0×10^{-3}	1.1×10^{-3}	1.3×10^{-4}	5.0×10^{-3}
CH5	59.87	0.83	3.2×10^{-3}	1.4×10^{-3}	1.3×10^{-4}	4.5×10^{-2}
CH7	32.09	2.6	3.2×10^{-3}	1.0×10^{-2}	1.3×10^{-4}	3.2×10^{-3}
CH8	29.9	1.8	3.2×10^{-3}	2.5×10^{-3}	1.3×10^{-4}	1.4×10^{-2}
CH10	29.61	2.49	3.2×10^{-3}	6.9×10^{-4}	1.3×10^{-4}	1.3×10^{-2}
CH10-L	29.32	2.43	3.2×10^{-3}	3.0×10^{-3}	1.3×10^{-4}	1.0×10^{-2}
CH10-S	31.77	2.46	3.2×10^{-3}	7.2×10^{-4}	1.3×10^{-4}	1.3×10^{-2}
CH11	30.21	3.91	3.2×10^{-4}	4.1×10^{-5}	1.3×10^{-4}	6.3×10^{-3}
CH12	5.87	2.57	1.5×10^{-3}	4.1×10^{-5}	1.3×10^{-4}	5.6×10^{-3}
CH13	7.93	2.07	3.2×10^{-3}	3.1×10^{-4}	1.3×10^{-4}	7.1×10^{-3}
CH14	17.89	2.45	2.7×10^{-3}	3.6×10^{-3}	1.3×10^{-4}	5.0×10^{-3}
CH15	44.68	2.27	3.2×10^{-3}	7.4×10^{-4}	1.3×10^{-4}	1.4×10^{-2}
CH16	55.81	1.05	2.7×10^{-3}	1.3×10^{-4}	1.3×10^{-4}	2.2×10^{-2}
CH17	79.16	0.47	3.2×10^{-3}	7.4×10^{-4}	1.3×10^{-4}	2.8×10^{-2}
Geometric mean			2.5×10^{-3}	8.4×10^{-4}	1.3×10^{-4}	9.7×10^{-3}

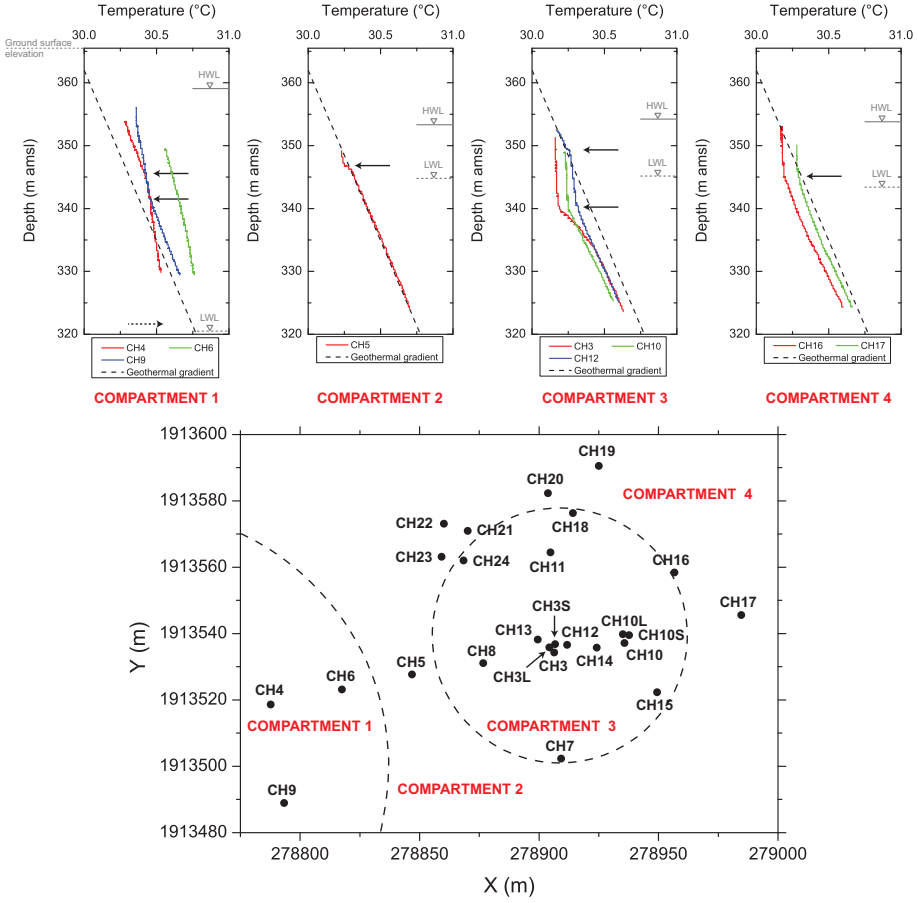

Fig. 10. Hydraulic compartmentalization of the aquifer under low water level conditions (LWL) related to the location of deeper flowing fractures in the EHP thanks to temperature logging carried out under high water level conditions (HWL). Map is in the UTM projected coordinate system.

fined, as is the case between compartments 2 and 4. However, under low water level conditions, the different compartments are disconnected from each other. Note that the changes in temperature with depth are also consistent within each compartment (Fig. 10).

All this information is summarized in Fig. 11 as a detailed hydrogeological conceptual model at the site scale. This shows that the first flowing fractured zone, located in the upper part of the granite, is laterally well-connected throughout the site. This fractured zone is also well-connected with the bottom of the saprolite (Boisson et al., in preparation). Thus, under high water level conditions, all the boreholes are connected through the fracture network located in the upper part of the granite, in the few first meters below the saprolite. During low water level conditions, the boreholes remain connected if they intersect common deeper flowing fractures. Interestingly, the main flowing fractures within each compartment are located at approximately the same level. The limited extension of deeper flowing fractures results in hydraulic compartmentalization of the aquifer.

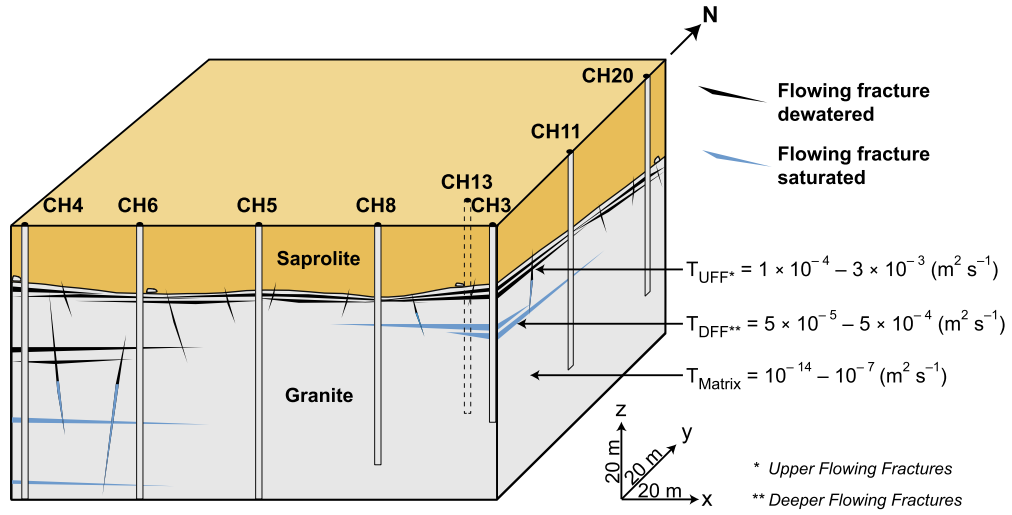

Fig. 11. Hydrogeological conceptual model of the EHP under low water level conditions, where only the deeper flowing fractures are saturated. Upper flowing fractures are figured in dewatered conditions. The range of transmissivities is also provided for upper and deeper flowing fractures.

The estimated transmissivity of the main upper fractured zone varies from 1×10^{-4} to 3×10^{-3} m^2 s^{-1} whereas the transmissivity of the deeper fractured zones is lower, with values ranging from 5×10^{-5} to 5×10^{-4} m^2 s^{-1}. The storage coefficient of the aquifer is also variable with higher values under high water level conditions (Tables 4–6). Although some values were certainly over-estimated or under-estimated due to the frequent difficulty of estimating the storage coefficient, especially in heterogeneous media (Meier et al., 1998), the saprolite should ensure storage while the fractures ensure the transmissive role of the aquifer (Chilton and Foster, 1995; Taylor and Howard, 2000; Maréchal et al., 2004; Dewandel et al., 2006). This indicates that the low water level below the saprolite represents critical conditions for the exploitation of groundwater resources.

5. Discussion

In the previous sections, we showed that the main transmissive and connected zone consists of a fractured zone a few meters thick, located below the saprolite on top of the fractured granite. Some permeable fractures may also be encountered at greater depths, up to 60 m, but with generally lower transmissivity and limited extension and continuity. In consequence, the geometry of this upper fractured zone will partly control the hydrology of the watershed. In particular, this explains why groundwater may flow over the entire watershed when the water level is sufficiently high whereas it may be restricted to a few compartments when the water level is below this permeable structure. Thus, groundwater flow is highly dependent on the depth of this interface in the watershed, which is highly variable.

Some outcrops of fresh or poorly fractured granite are present in many places within the watershed, clearly showing that this fractured zone is not present throughout the watershed. Fig. 12 provides a schematic diagram of the potential geometry of this fractured zone in such a context, where its interruption can be due to the presence of inselbergs or very poorly fractured granite outcrops within the watershed. The hydrologic conditions are represented for two different states: under high water level conditions (Fig. 12a) and under low water level conditions (Fig. 12b). The permeable saturated reservoirs are also represented although their extension and complexity remains uncertain. In this model, the well-connected transmissive zone is constituted by the interface between saprolite and granite and by the first few flowing fractures observed in the upper part of the granite. The fracture network is certainly more complex in reality but, in this conceptual model, we simplify fracture geometry to the main flowing fracture zones. The well-connected transmissive zone mainly drives the

Table 6
Computed parameters with $R = 12$ m for pumping test performed in the CH11 borehole at low water level conditions in January 2013.

Name of borehole	Distance from pumping borehole (m)	s_{max} (m)	T_1 (m^2 s^{-1})	S_1 (–)	T_2 (m^2 s^{-1})	S_2 (–)
CH3	30.21	2.14	3.4×10^{-4}	5.7×10^{-4}	4.9×10^{-5}	8.9×10^{-6}
CH5	68.64	No reaction	–	–	–	–
CH7	62.29	1.86	3.4×10^{-4}	5.7×10^{-4}	4.9×10^{-5}	7.1×10^{-6}
CH8	43.68	2.06	3.4×10^{-4}	8.2×10^{-4}	4.9×10^{-5}	7.1×10^{-6}
CH10	41.33	1.88	3.4×10^{-4}	6.2×10^{-4}	4.9×10^{-5}	1.4×10^{-5}
CH11	Pumping borehole	2.28	3.4×10^{-4}	1.3×10^{-3}	4.9×10^{-5}	1.3×10^{-4}
CH12	28.71	2.14	3.4×10^{-4}	6.8×10^{-4}	4.9×10^{-5}	8.9×10^{-6}
CH13	26.81	2.12	3.4×10^{-4}	5.7×10^{-4}	4.9×10^{-5}	1.3×10^{-5}
CH14	34.62	1.94	3.4×10^{-4}	9.0×10^{-4}	4.9×10^{-5}	1.4×10^{-5}
CH15	61.36	1.68	3.4×10^{-4}	3.3×10^{-4}	4.9×10^{-5}	1.6×10^{-5}
CH16	52.23	No reaction	–	–	–	–
CH17	82.1	No reaction	–	–	–	–
CH18	15.13	2.1	3.4×10^{-4}	5.7×10^{-4}	4.9×10^{-5}	3.5×10^{-5}
CH19	33.03	No reaction	–	–	–	–
CH20	17.91	No reaction	–	–	–	–
Geometric mean			3.4×10^{-4}	6.5×10^{-4}	4.9×10^{-5}	1.5×10^{-5}

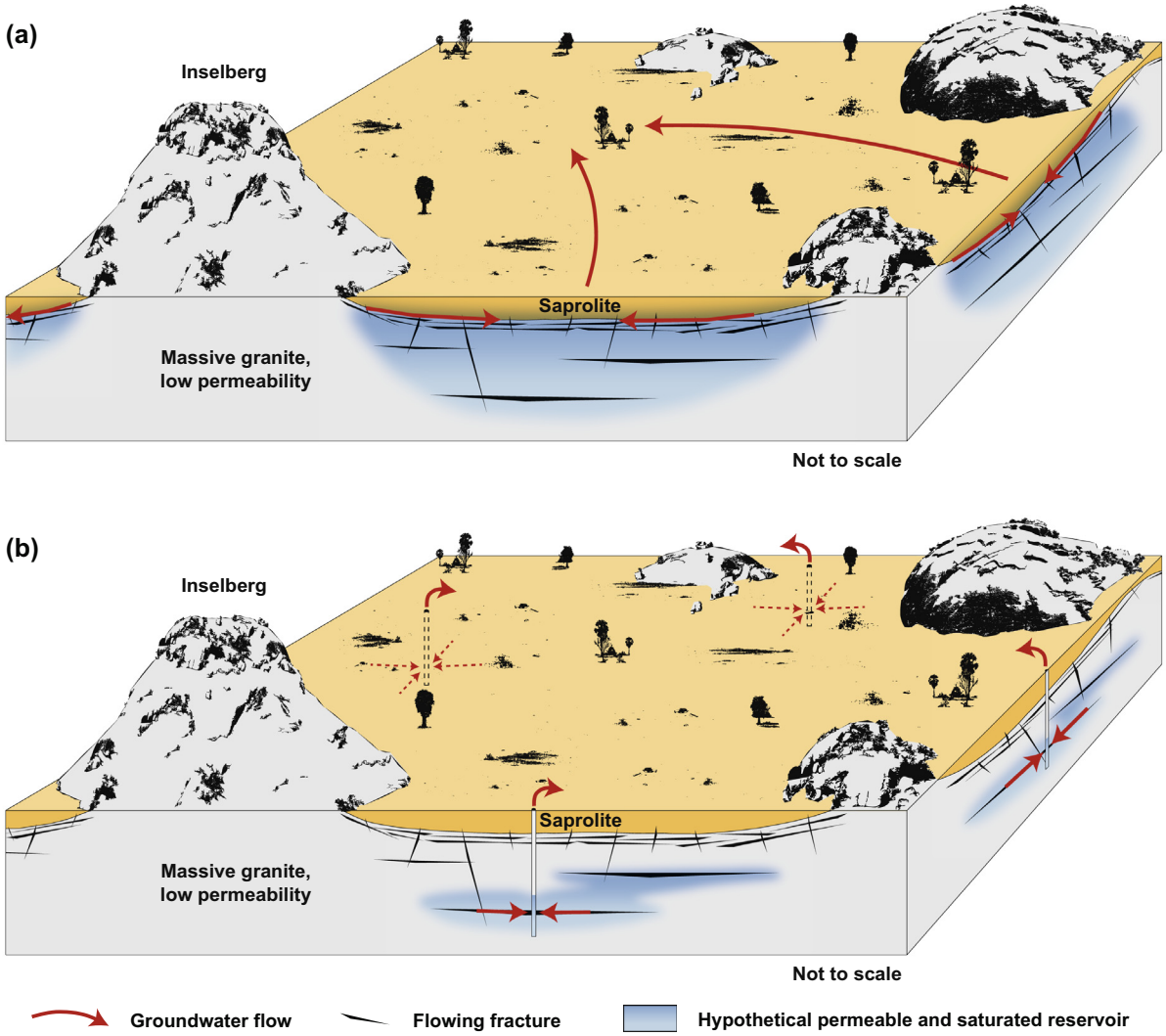

Fig. 12. Conceptual groundwater flow model at the watershed-scale as a function of water level conditions: (a) under high water level conditions and (b) under low water level conditions.

groundwater flows under high water level conditions despite the presence of some inselbergs (Fig. 12a). During low water level conditions, the groundwater flows are mostly restricted to compartments and the aquifer is partially disconnected at the watershed scale (Fig. 12b). Depending on the water level, the groundwater flow shifts from a watershed flow system to local almost independent flow systems.

Other studies performed in the same region focused on the compartmentalization of the watershed due to geological structures such as a dyke (Perrin et al., 2011a) or quartz reef (Dewandel et al., 2011). We show here that the hydraulic compartmentalization in such media can also be linked to the limited extension of the deeper flowing fractures. Based on the borehole data and piezometric maps in Fig. 5, the estimated length of the deeper flowing fractured zone is typically around one hundred meters in the main part of the site (i.e. compartment 3, Fig. 10). Our estimation of the size of the compartments is consistent with reports showing that fracture length may attain more than hundred meters in such media (Hencher et al., 2011). To provide an order-of-magnitude of the characteristic length of these compartments, Fig. 13 shows the variograms for the two piezometric maps obtained under high water level conditions (2011) and low water level conditions (2013) by applying the GDM tool (BRGM software, GDM, 2001). Such variograms are classically used in geostatistics to analyse the spatial structuration of a given variable. In particular, it can be used to estimate the characteristic distance (“range”) between the variable measurement locations over which the variable is not spatially correlated. The variogram under low water level conditions shows an estimated characteristic length of 345 m (range on spherical model – Fig. 13) whereas no characteristic length could be estimated under high water level conditions, because of the topographic control of the piezometric map at the watershed-scale. Interestingly, a similar length (500 m) was found by Dewandel et al. (2012) during upscaling of hydraulic properties in analogous fractured granite in Andhra Pradesh and by Perrin et al. (2011a) based on hydrochemical signatures of aquifer compartments (400–500 m).

Identification of the upper well-connected fractured zone as the main hydrogeological structure in the watershed is consistent with other studies carried out in similar weathered and fractured media. Most authors agree about the existence of a more permeable zone at the interface between the saprolite and the granite and in the upper part of the fractured granite (Larsson, 1984; Jones, 1985; Acworth, 1987; Howard et al., 1992; Chilton and Foster, 1995; Wyns et al., 2004; Dewandel et al., 2006). The depth of this zone or interface is expected to vary from place to place due to the variations of weathering intensity or hardness of granite. This observation is also consistent with the geophysical imaging carried out by Braun et al. (2009) at the Mule Hole site on the Karnataka plateau which revealed the variable depth of the saprolite. Despite some possible

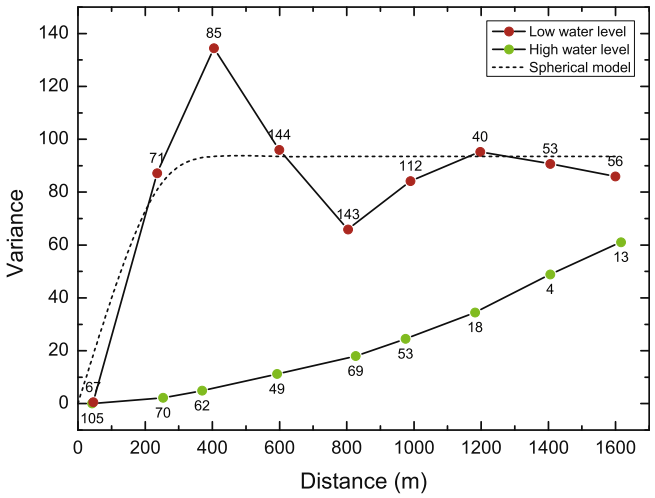

Fig. 13. Variograms obtained for both piezometric maps at watershed scale under high water level conditions (2011) and under low water level conditions (2013) with spherical model.

variations in the thickness of the saprolite or depth of the main permeable zone, this groundwater conceptual model is expected to be also representative of other regions of India as at Maheshwaram (Maréchal et al., 2004; Dewandel et al., 2006) or in other areas also affected by sub-surface weathering and fracturing processes. Of course, the sensitivity to water level conditions will depend on both climate and anthropogenic pressure.

This hydrogeological conceptual model, which highlights the compartmentalization of the aquifer, should be taken into account in future groundwater and transport modeling of such media. The respective roles of the different fractured zones on groundwater flows will require an appropriate approach to take into account the specific heterogeneities (Sanchez-Vila et al., 1996; Hsieh, 1998). This is especially true for the prediction of contaminant transport where the connectivity of fractures will clearly affect time transfer and chemical processes including water rock-interaction. This hydrogeological model also implies a compartmentalization of residence times and groundwater ages (Ayraud et al., 2008). On the one hand, relatively short residence times should be expected due to low storage (Dewandel et al., 2012). But, on the other hand, much higher residence times should be expected in the deeper part of each compartment, in particular in deeper permeable fractures in which the hydraulic connections are poor. The water level conditions may also have major impacts on groundwater chemistry, especially when the watershed becomes somehow endorheic under low water level conditions. These changes in watershed hydrology may partly explain certain enrichments in anthropogenic or geogenic pollutants, such as Fluoride, which have dramatically increased since the last ten years in Southern India (Perrin et al., 2011b; Pettenati et al., 2013).

More generally, this case study highlights the vulnerability of such groundwater resources to anthropogenic impacts and climate variability. In the present case, the critical situations encountered under low water level conditions led many farmers in the area to reduce watering and their irrigated rice cropping area. It also led to some agricultural changes with the development of crop lentils or cotton rather than rice. The boreholes of some farmers became dry due to the decline of water levels. This shows the need for groundwater management and protection in this area, in particular, in a country where demographic pressure is still increasing significantly and where groundwater resources are, in most Indian places, the main available water resource. The hydrogeological conceptual model proposed here illustrates how groundwater resources depend on the hydraulic connectivity of fractures which controls groundwater flows at local and watershed scales. Such a conceptual groundwater flow model may be of great help to better locate boreholes of higher productivity although productivity depends on fracture hydraulic properties which are highly variable in the sub-surface. It may allow also to define a critical depth for water level below which groundwater supply will depend only on local and limited resources. In addition, the knowledge of water levels combined with saprolite's depth at the watershed or regional scale, may allow to better analyze the possible interconnection within or between watersheds for improving management and protection of groundwater resources. This will be certainly the topics of future studies.

6. Conclusion

This study of a shallow fractured crystalline aquifer shows a discontinuous hydrogeological system, which is revealed by low water level conditions. By focussing on fracture network connectivity, we were able to highlight the compartmentalization of the system. First, we showed that the permeable zone including the bottom of the saprolite and the upper part of the granite is laterally well-connected. At the watershed scale, groundwater flows mainly through this permeable zone. Then, we demonstrated that the hydraulic connectivity of fractures strongly decreases with depth and the limited extension of the deeper flowing fractures leads to a lateral compartmentalization of the aquifer when the groundwater level decreases. Depending on the water level conditions, the aquifer shifts from a watershed flow system to independent local flow systems.

This understanding of groundwater flows in such a context is of prime importance for sustainable aquifer management, in particular, in a country where demographic pressure is still increasing significantly and where groundwater constitutes the main available water resource. Such changes in groundwater flows illustrate the vulnerability of rural communities in the area regarding the perennial access to groundwater resource for drinking water and irrigation purposes. This also illustrates the impacts of anthropogenic pressure and climate variability on groundwater resources availability. This hydrogeological compartmentalization, without any flow at the watershed scale under low water level conditions, has surely a significant impact on groundwater chemistry and contaminant transport which deserves specific investigations. Further work is needed to analyse in more details the link between hydrology and hydrochemistry at the watershed scale under these particular conditions. Of particular interest will be groundwater dating which should also reveal compartmentalization within the watershed as a function of depth. It will also be of interest to use geophysical imagery to investigate the specific morphology of the compartments at depth, in greater detail and in different areas.

Acknowledgements

This study has been carried out at the Indo-French Centre for Groundwater Research (BRGM-NGRI). This work has mainly benefited from CARNOT Institute BRGM funding. The Choutuppal Experimental Hydrogeological Park has also benefited from INSU support within the H+ observatory. The authors are very grateful to Mohammed Wajiduddin, David Villesseche, Irshad Hussain, Yata Muthyalu and Yata Ramesh for the field work and to Bernard Bourgine for geostatistical analysis. The authors also thank very much two anonymous reviewers and the associate editor for their very constructive and fruitful comments that greatly enhance the quality of the manuscript.

References

Acworth, R.I., 1987. The development of crystalline basement aquifers in a tropical environment. Q. J. Eng. Geol. 20, 265–272.

Akkiraju, V.V., Roy, S., 2011. Geothermal climate change observatory in south India 1: borehole temperatures and inferred surface temperature histories. Phys. Chem. Earth, Parts A/B/C 36, 1419–1427.

Anand, R.R., Paine, M., 2002. Regolith geology of the Yilgarn Craton, Western Australia: implications for exploration. Aust. J. Earth Sci. 49 (1), 3–162.

Ayoob, S., Gupta, A.K., 2006. Fluoride in drinking water: a review on the status and stress effects. Crit. Rev. Environ. Sci. Technol. 36, 433–487.

Ayraud, V., Aquilina, L., Labasque, T., Pauwels, H., Molenat, J., Pierson-Wickmann, A.-C., Durand, V., Bour, O., Tarits, C., Le Corre, P., Fourre, E., Merot, P., Davy, P., 2008. Compartmentalization of physical and chemical properties in hard-rock aquifers deduced from chemical and groundwater age analyses. Appl. Geochem. 23, 2686–2707.

Bahat, D., Grossenbacher, K., Karasaki, K., 1999. Mechanism of exfoliation joint formation in granitic rocks, Yosemite National Park. J. Struct. Geol. 21, 85–96.

Banks, E.W., Simmons, C.T., Love, A.J., Cranswick, R., Werner, A.D., Bestland, E.A., Wood, M., Wilson, T., 2009. Fractured bedrock and saprolite hydrogeologic controls on groundwater/surface-water interaction: a conceptual model (Australia). Hydrogeol. J. 17, 1969–1989.

Barker, J., 1988. A generalized radial flow model for hydraulic tests in fractured rock. Water Resour. Res. 24, 1796–1804.

Bour, O., Davy, P., 1998. On the connectivity of three-dimensional fault networks. Water Resour. Res. 34, 2611–2622.

Bourdet, D., Whittle, T.M., Douglas, A.A., Pirard, Y.M., 1983. A new set of type curves simplifies well test analysis. World Oil 196, 95–101.

Bouwer, H., Rice, R.C., 1976. Slug test for determining hydraulic conductivity of unconfined aquifers with completely or partially penetrating wells. Water Resour. Res. 12, 423–428.

Braun, J.-J., Descloitres, M., Riotte, J., Fleury, S., Barbiero, L., Boeglin, J.-L., Violette, A., Lacarce, E., Ruiz, L., Sekhar, M., Kumar, M.S.M., Subramanian, S., Dupre, B., 2009. Regolith mass balance inferred from combined mineralogical, geochemical and geophysical studies: Mule Hole gneissic watershed, South India. Geochim. Cosmochim. Acta 73, 935–961.

Briz-Kishore, B.H., 1993. Assessment of yield characteristics of granitic aquifers in South India. Ground Water 31, 921–928.

Butler, J., 1988. Pumping tests in nonuniform aquifers – the radially symmetric case. J. Hydrol. 101, 15–30.

Chatelier, M., Ruelleu, S., Bour, O., Porel, G., Delay, F., 2011. Combined fluid temperature and flow logging for the characterization of hydraulic structure in a fractured karst aquifer. J. Hydrol. 400, 377–386.

Chilton, P., Foster, S., 1995. Hydrogeological characterisation and water-supply potential of basement aquifers in tropical Africa. Hydrogeol. J. 3, 36–49.

Courtois, N., Lachassagne, P., Wyns, R., Blanchin, R., Bougaire, F.D., Some, S., Tapsoba, A., 2010. Large-scale mapping of hard-rock aquifer properties applied to Burkina Faso. Ground Water 48, 269–283.

Dale, T., 1923. The commercial granites of New England. United States Geological Survey, Bulletin 738, U.S. Government Printing Office, Book, p. 488.

Day-Lewis, F.D., Hsieh, P.A., Gorelick, S.M., 2000. Identifying fracture-zone geometry using simulated annealing and hydraulic-connection data. Water Resour. Res. 36, 1707–1721.

de Dreuzy, J., Davy, P., Bour, O., 2001. Hydraulic properties of two-dimensional random fracture networks following a power law length distribution 1. Effective connectivity. Water Resour. Res. 37, 2065–2078.

Dewandel, B., Lachassagne, P., Wyns, R., Maréchal, J.C., Krishnamurthy, N.S., 2006. A generalized 3-D geological and hydrogeological conceptual model of granite aquifers controlled by single or multiphase weathering. J. Hydrol. 330, 260–284.

Dewandel, B., Perrin, J., Ahmed, S., Aulong, S., Hrkal, Z., Lachassagne, P., Samad, M., Massuel, S., 2010. Development of a tool for managing groundwater resources in semi-arid hard rock regions: application to a rural watershed in South India. Hydrol. Process. 24, 2784–2797.

Dewandel, B., Lachassagne, P., Zaidi, F.K., Chandra, S., 2011. A conceptual hydrodynamic model of a geological discontinuity in hard rock aquifers: example of a quartz reef in granitic terrain in South India. J. Hydrol. 405, 474–487.

Dewandel, B., Maréchal, J.C., Bour, O., Ladouche, B., Ahmed, S., Chandra, S., Pauwels, H., 2012. Upscaling and regionalizing hydraulic conductivity and effective porosity at watershed scale in deeply weathered crystalline aquifers. J. Hydrol. 416, 83–97.

Drury, M., 1984. Borehole temperature logging for the detection of water-flow. Geoexploration 22, 231–243.

Foster, S.S.D., 1984. African groundwater development - the challenges for hydrogeological science. IAHS Publication 144, 3–12.

G.S.I., 1999. Resources map of Nalgonda district, Andhra Pradesh. Geological and Minerals. Geological Survey of India.

G.S.I., 2005. Geological and Mineral map of Andhra Pradesh. Geological Survey of India.

GDM, 2001. Geological information – modeling and display. Technical features of version 7.0. <http://gdm.brgm.fr>.

Gringarten, A.C., 2008. From straight lines to deconvolution: the evolution of the state of the art in well test analysis. SPE Reservoir Eval. Eng. 11, 41–62.

Gustafson, G., Krásný, J., 1994. Crystalline rock aquifers: their occurrence, use and importance. Appl. Hydrogeol. 2, 64–75.

Hencher, S.R., Lee, S.G., Carter, T.G., Richards, L.R., 2011. Sheeting joints: characterisation, shear strength and engineering. Rock Mech. Rock Eng. 44, 1–22.

Houston, J., Lewis, R., 1988. The Victoria-Province drought relief project, II Borehole yield relationships. Ground Water 26, 418–426.

Howard, K.W.F., Hughes, M., Charlesworth, D.L., Ngobi, G., 1992. Hydrogeologic evaluation of fracture permeability in crystalline basement aquifers of Uganda. Appl. Hydrogeol. 1, 55–65.

Hsieh, P.A., 1998. Scale effects in fluid flow through fractured geologic media, Scale Dependence and Scale Invariance in Hydrology. Cambridge University Press.

Jahns, R., 1943. Sheet structure in granites its origin and use as a measure of glacial erosion in New England. J. Geol. 51, 71–98.

Jones, M., 1985. The weathered zone aquifers of the basement-complex areas of Africa. Q. J. Eng. Geol. 18, 35–46.

Keys, W.S., 1990. Borehole geophysics applied to ground-water investigations. In: USGS (Ed.), Techniques of Water-Resources Investigations of the United States Geological Survey, Book 2, p. 150.

Klepikova, M.V., Le Borgne, T., Bour, O., Davy, P., 2011. A methodology for using borehole temperature-depth profiles under ambient, single and cross-borehole pumping conditions to estimate fracture hydraulic properties. J. Hydrol. 407, 145–152.

Larsson, I., 1984. Ground water in hard rocks: project 8.6 of the International Hydrological Programme, vol. 33 of Studies and reports in hydrology. UNESCO publication.

Le Borgne, T., Bour, O., de Dreuzy, J., Davy, P., Touchard, F., 2004. Equivalent mean flow models for fractured aquifers: Insights from a pumping tests scaling interpretation. Water Resour. Res. 40, 1–12.

Le Borgne, T., Bour, O., Paillet, F.L., Caudal, J.P., 2006. Assessment of preferential flow path connectivity, and hydraulic properties at single-borehole and cross-borehole scales in a fractured aquifer. J. Hydrol. 328, 347–359.

Maréchal, J.-C., 2010. Editor's message: the sunk cost fallacy of deep drilling. Hydrogeol. J. 18, 287–289.

Maréchal, J.C., Wyns, R., Lachassagne, P., Subrahmanyam, K., Touchard, F., 2003. Vertical anisotropy of hydraulic conductivity in fissured layer of hard-rock aquifers due to the geological structure of weathering profiles. C.R. Geosci. 335, 451–460.

Maréchal, J.C., Dewandel, B., Subrahmanyam, K., 2004. Use of hydraulic tests at different scales to characterize fracture network properties in the weathered-fractured layer of a hard rock aquifer. Water Resour. Res. 40, W11508.

Maréchal, J.C., Dewandel, B., Ahmed, S., Galeazzi, L., Zaidi, F.K., 2006. Combined estimation of specific yield and natural recharge in a semi-arid groundwater basin with irrigated agriculture. J. Hydrol. 329, 281–293.

Meier, P., Carrera, J., Sanchez-Vila, X., 1998. An evaluation of Jacob's method for the interpretation of pumping tests in heterogeneous formations. Water Resour. Res. 34, 1011–1025.

National Research Council, 1996. Rock Fractures and Fluid Flow: Contemporary Understanding and Applications. The National Academies Press, Washington, D.C., p. 551.

Paillet, F.L., 1998. Flow modeling and permeability estimation using borehole flow logs in heterogeneous fractured formations. Water Resour. Res. 34, 997–1010.

Perrin, J., Ahmed, S., Hunkeler, D., 2011a. The effects of geological heterogeneities and piezometric fluctuations on groundwater flow and chemistry in a hard-rock aquifer, southern India. Hydrogeol. J. 19, 1189–1201.

Perrin, J., Mascre, C., Pauwels, H., Ahmed, S., 2011b. Solute recycling: an emerging threat to groundwater quality in southern India? J. Hydrol. 398, 144–154.

Pettenati, M., Perrin, J., Pauwels, H., Ahmed, S., 2013. Simulating fluoride evolution in groundwater using a reactive multicomponent transient transport model: application to a crystalline aquifer of Southern India. Appl. Geochem. 29, 102–116.

Pira, K., 2009. Characterization of the Experimental Hydrogeological Park (Choutuppal, India). Master thesis, University of Montpellier 2, France (in French).

Reddy, D.V., Nagabhushanam, P., Sukhija, B.S., Reddy, A.G.S., 2009. Understanding hydrological processes in a highly stressed granitic aquifer in southern India. Hydrol. Process. 23, 1282–1294.

Renard, P., Glenz, D., Mejias, M., 2009. Understanding diagnostic plots for well-test interpretation. Hydrogeol. J. 17, 589–600.

Sanchez-Vila, X., Carrera, J., Girardi, J., 1996. Scale effects in transmissivity. J. Hydrol. 183, 1–22.

Shah, T., Roy, A., Qureshi, A., Wang, J., 2003. Sustaining Asia's groundwater boom: an overview of issues and evidence. Nat. Resour. Forum 27, 130–141.

Shapiro, A., Hsieh, P., 1998. How good are estimates of transmissivity from slug tests in fractured rock? Ground Water 36, 37–48.

Taylor, R., Howard, K., 2000. A tectono-geomorphic model of the hydrogeology of deeply weathered crystalline rock: evidence from Uganda. Hydrogeol. J. 8, 279–294.

Twidale, C.R., 1973. On the origin of sheet jointing. Rock Mech. 5, 163–187.

Vidal Romaní, J., Twidale, C., 1999. Sheet fractures, other stress forms and some engineering implications. Geomorphology 31, 13–27.

Wright, E.P., 1992. The hydrogeology of crystalline basement aquifers in Africa. In: Wright, E.P., Burgess, W. (Eds.), Hydrogeology of crystalline basement aquifers in Africa, vol. 66. London Special Publication, pp. 1–27.

Wyns, R., Baltassat, J., Lachassagne, P., Legchenko, A., Vairon, J., Mathieu, F., 2004. Application of proton magnetic resonance soundings to groundwater reserve mapping in weathered basement rocks (Brittany, France). Bull. Soc. Géol. France 175, 21–34.